Modeling Pore Pressure Evolution in Organic Shale under the Effect of Maturation

Xuan Qin[1]*, De-hua Han[1], and Luanxiao Zhao[2,1], [1]University of Houston, [2]Tongji University

Summary

We devise a workflow to model the pore pressure increase in organic shale to better characterize the shale reservoirs. In particular, the proposed model considers the microstructure in organic shale and the volume fraction variations of rock components during the maturation. The pore pressure increase is solved based on the compressibility and volumes of pore space and pore fluids. Our modeling results agree that the evolution of organic shale's rock-physics property during kerogen maturation is consistent with fluid expansion model that sonic velocity decrease while density changes little when unloading occurs.

Introduction

Pore pressure prediction in shale has been extensively studied, but most studies focus on the overpressure caused by the mechanism of disequilibrium compaction during the loading (compaction) process. The organic shale has become our interest because it is both a hydrocarbon source rock and a reservoir rock. Studying pore pressure in organic shale can reflect the status of pore fluid existence, type, accumulation and ensure drilling safety. However, due to the presence and maturation process of kerogen, a form of amorphous organic matter, it is challenging to characterize pore pressure accumulation and the elastic property in organic shales.

Some authors have predicted and analyzed organic shale's elastic properties. Carcione et al. (2011) found a dependence of velocity on total organic carbon (TOC) when modeling oil-saturated rock using the Backus average and the Krief/Gassmann models. Vernik and Milovac (2011) and Zhu et al. (2012) found that TOC tends to decrease the P- and S-wave velocities, density, and Vp/Vs ratios, while increasing the velocity anisotropies. Lucier et al. (2011) showed that, in the Haynesville shale gas reservoir, the effect of gas saturation on the Vp-Vs relation is more significant than the impacts of TOC. Guo et al. (2013) modeled Barnett shale brittleness index with self-consistent approximations and the Backus average by considering the degree of the preferred orientation of clay and kerogen particles. Qin et al. (2014) and Zhao et al. (2016) established modeling framework to characterize organic shale stiffness based on the analysis of each component's geometry and load-bearing material. However, little work has considered the concomitant pore pressure generation while describing the elastic property of organic shale.

Effects of Kerogen Morphology and TOC

To explicit model the organic shale's composition and structure, we study the porous structure of with SEM images in Figure 1. The overmature Woodford shale in gas-window and has a vitrinite reflectance (Ro) at 1.5%, and its TOC is 6.2%. In Figure 1a, we observe the rounded pores in the dispersed kerogen bodies filled in the inorganic matrix. In Figure 1b, only smaller domains of organic matter are porous (marked by white arrows), while the larger domains in sheet-like shape are non-porous and appear homogeneous, which may have been compacted during maturation. Therefore, we hypothesize that the kerogen pores tend to be open when organic matter is dispersed and filled in the shale matrix or closed when organic matter is lenticular and supports the rock matrix.
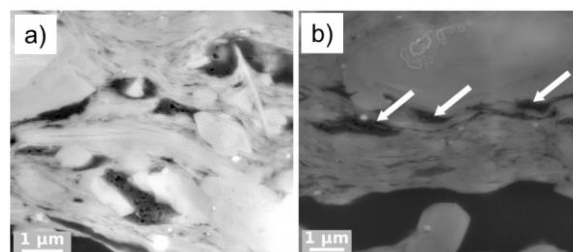

Figure 1. SEM images of the overmature Woodford shale (Löhr et al., 2014). a) round pores exist in dispersed organic matter bodies; b) no pores exist in sheet-like organic matter.

If we make a further investigation, there may be a threshold of TOC value that determines the morphology and role of organic matter in organic shales. In Figure 2a, Milliken et al. (2013) plotted the porosity and TOC of the Marcellus shale samples from two wells. The diamond symbols denote samples in Well 1 with an average depth around 1500 m and lower Ro at 1%. The square symbols denote samples in Well 2 with an average depth around 2800 m and higher Ro at 2.1%. The samples in two wells have a similar TOC range, and the relationship between porosity and TOC is noteworthy. A threshold of TOC at 5.6% is selected to divide shales into two groups, where the filled symbols represent samples with a TOC less than 5.6%, and the unfilled symbols represent samples with a TOC larger than 5.6%. When TOC is less than 5.6%, porosity increases with TOC and the slopes in two wells are approximately the same. The two linear trends' interceptions (when TOC = 0) are different in two wells, indicating that the mineral porosities are 3% in Well 1 or 1% in Well 2 and cause the differences in porosities at the same TOC. It suggests that the organic matter pore is less affected by compaction due to stiff rock frame if kerogen is part of pore-filling. When TOC is higher than 5.6%, porosity stops increasing with the TOC. Specifically, porosity drops with the increase in TOC for Well 1 with lower maturity;

porosity increases with the rise in TOC for Well 2 with higher maturity. Porosity can be seen as a function of maturation and compaction.
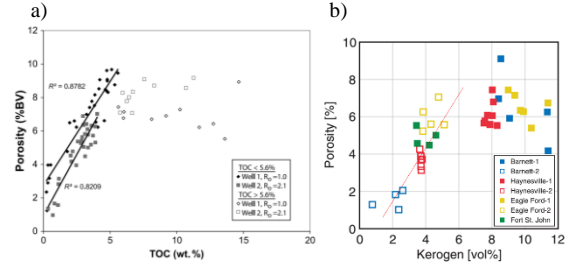

Figure 2. Porosity varies with organic matter richness. a) data are from two wells of the Marcellus shale (Miliken et al., 2013); b) data are from different shale samples (Sone and Zoback, 2013).

A similar pattern can be observed in Figure 2b. Samples are from different unconventional shale reservoirs (Sone and Zoback, 2013), and a threshold of kerogen volume fraction is near 6%. Filled symbols in Figure 2b represent samples with higher clay content and higher organic matter richness, compared with samples in unfilled symbols and the same color. So if organic shale's TOC is above the threshold value, the organic matter tends to be in a layered structure or lenticular shape, and the total porosity does not relate with TOC. So in Table 1, we propose that a threshold TOC controls the shape and role of organic matter (OM) in shale, which is considered in the following modeling framework.

Table 1. A threshold of TOC value dominates the organic matter morphology and role in organic shales.

TOC (wt.%)	OM shape	OM role in shale
< 5.6	Spherical/dispersed	Pore-filling
> 5.6	Lenticular/layered	Load-bearing

Modeling Workflow

Step I: Bulk Volume Model
We illustrate the bulk volume model for organic shale in Figure 3. Organic shale consists of kerogen part (V_k) and non-kerogen part (V_{nk}) with the sum of their volume fractions as one. The kerogen part consists of solid kerogen and organic matter pores, while the non-kerogen part is composed of inorganic minerals and mineral pores (Alfred and Vernik, 2012; Milliken et al., 2013). So the total porosity equals the sum of kerogen-related porosity and non-kerogen-related porosity ($\phi_t = \phi_k + \phi_{nk}$). The solid density ρ_m is expressed as

$$\rho_m = K\rho_k + (1-K)\rho_{nk}, \quad (1)$$

where K and $1-K$ are the volume fractions of solid kerogen and inorganic mineral in shale matrix, ρ_k and ρ_{nk} are the

densities of solid kerogen and mineral (a mixture of clay, quartz, carbonates, etc.).
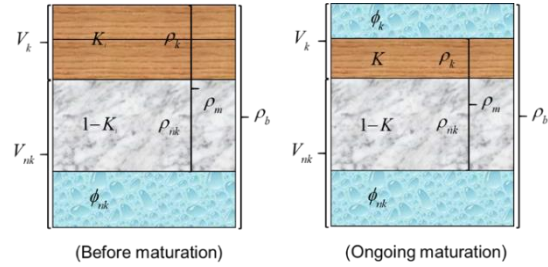

Figure 3. Bulk volume model of organic shale.

The volume fraction of solid organic matter in the matrix (K) relates to TOC through

$$TOC = KC_k\rho_k / \rho_m, \quad (2)$$

$$K = TOC \cdot \rho_{nk} / [C_k\rho_k + TOC \cdot (\rho_{nk} - \rho_k)], \quad (3)$$

where C_k represent the carbon weight fraction in organic matter, usually ranging from 0.7 to 0.85 with increasing maturity (Vernik and Milovac, 2011). Therefore, we can estimate TOC value with above equations by given kerogen density, matrix density, and inorganic mineral density.

When environmental temperature is over 50 °C, kerogen in organic shale becomes thermally unstable and starts to decompose to generate hydrocarbons such as oil and gas. If the TOC is less than the threshold, e.g., 5.6%, and the organic matter is mostly dispersed or spherical as pore-filling, the organic matter pores remain open after the decomposition of kerogen due to the stiff rock frame. With a transformation ratio of kerogen F, the kerogen-related porosity can be expressed by

$$\phi_k = (1-\phi_{nk})K_i F, \quad (4)$$

where subscript "K_i" represents the initial value of the solid kerogen volume fraction in the solid part of shale.

We have the volume fraction of other components (minerals and solid organic matter) in bulk rock as

$$V_{\text{mineral}} = (1-\phi_{nk})(1-K_i), \quad (5)$$

$$V_{om} = (1-\phi_{nk})K_i(1-F). \quad (6)$$

If the TOC is larger than the threshold and organic matter is part of the load-bearing material, the generated space within kerogen tends to be more compacted and does not change much with TOC. So we have the kerogen-related porosity close to a constant, e.g., 4%, and volume fractions of mineral and solid organic matter and porosity can be expressed as

$$V_{\text{mineral}} = (1-\phi_k)(1-\phi_{nk0})(1-K_i)/(1-K_iF+K_iF\phi_{nk0}), (7)$$

$$V_{om} = (1-\phi_k)(1-\phi_{nk0})K_i(1-F)/(1-K_iF+K_iF\phi_{nk0}), (8)$$

$$\phi_{nk} = (1-\phi_k)\phi_{nk0}/(1-K_iF+K_iF\phi_{nk0}), \qquad (9)$$

where ϕ_k is assumed to be a constant. The bulk volume of the organic-rich shale can decrease during maturation:

$$V_T = (1-K_iF+K_iF\phi_{nk0})/(1-\phi_k). \qquad (10)$$

Step II: Modeling the Elastic Stiffness
Since we have introduced two types of bulk volume models for organic shale, we apply two strategies correspondingly in Figure 4 while modeling the stiffness of organic shale.
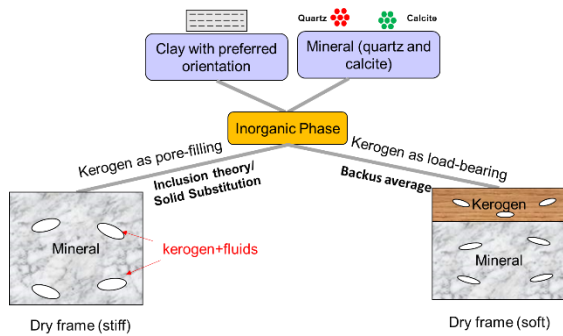

Figure 4. Schematic of modeling the stiffness of organic shale.

First, we model the stiffness of inorganic solid phase. The minerals of organic shale consist of clay, quartz, carbonates, etc., among which clay is treated as a transverse isotropic (TI) material (Tosaya, 1982; Sayers, 1994). We use the Self-Consistent Approximation (SCA) in the anisotropic domain (Hornby et al., 1994) to generate the stiffness of inorganic solid phase in shale, because it is unnecessary to identify a very type of mineral as the host material, and this algorithm considers the mineral's geometry through aspect ratio. In our modeling, quartz and carbonate have a spherical shape and clay has an elongated shape.

When TOC is low, and kerogen is pore-filling, by using Differential Effective Medium (DEM) method in the anisotropic domain (Nishizawa, 1982), we add zero modulus pore into the inorganic background to simulate the drained frame's elastic properties. The pore space contains the total volume of initial kerogen volume and mineral pore volume and has an ellipsoidal shape. Note that the pore-filling mixtures of kerogen, hydrocarbon, and water are not uniformly distributed and are considered as a patch mixing. Thus, the effective bulk and shear moduli of pore-filling are computed by the Voigt average (Domenico, 1976). At last, we use solid substitution equation (Ciz and Shapiro, 2007)

to add the mixture of solid kerogen and fluids into the drained frame.

When TOC is above the threshold and kerogen is load-bearing, we employ Backus average (Backus, 1962) to constitute a layered medium composed of organic and inorganic phases. The stiffness of water-saturated inorganic phase (non-kerogen part) can be modeled by adding water-filled pores into the inorganic background with DEM in the anisotropic domain (Nishizawa, 1982). The stiffness of hydrocarbon-saturated organic phase (kerogen part) can be modeled by adding hydrocarbon-filled pores into kerogen with Self-Consistent Approximation (Berryman, 1980).

Step III: Estimating Pore Pressure Increase
If solid kerogen cracks to generate hydrocarbon under a constant confining pressure, the volume of solid material decreases and fluid volume increases. Because the density of produced hydrocarbon (generally < 1 g/cm3) is less than solid kerogen (1.1~1.4 g/cm3) (Alfred and Vernik, 2012), the pore fluid volume increase is larger than the increase of pore space. We can solve the pore pressure increase based on the compressibility and volumes of pore filling and pore space.

When kerogen is not abundant and exists as a pore filling, the om pore is barely compacted, because the shale framework is stiff and the pore compressibility is low. During maturation, kerogen, hydrocarbon, and water exist in the pore space. Thus, we can expect a pore pressure increase ΔP to accommodate all the pore fillings in the pore space,

$$(V_k+\phi_{nk})(1+\beta_{pp}\Delta P)=(1-F)V_k(1-C_{om})\Delta P$$
$$+V_{wi}(1-C_w\Delta P)+V_{HC}(1-C_{HC}\Delta P) \qquad (11)$$

where $V_k+\phi_{nk}$, $(1-F)V_k$, V_{wi}, and V_{HC} represent the volume of pore space, remained solid kerogen, water, and hydrocarbon before pressure equilibrium, β_{pp} denotes the pore compressibility upon pore pressure change, C denotes material compressibility. And $V_{HC}=(1-E)FV_k\frac{\rho_k}{\rho_{HC}}$ is a function of the transformation ratio of kerogen (F) and expulsion/migration ratio of hydrocarbon (E). So we have

$$\Delta P=\frac{(1-E)F\frac{\rho_k}{\rho_{HC}}-F}{(\frac{\phi_{nk}}{V_k}+1)\beta_{pp}+(1-F)C_{om}+\frac{\phi_{nk}}{V_k}C_w+(1-E)F\frac{\rho_k}{\rho_{HC}}C_{HC}}. (12)$$

When the TOC is above the threshold, kerogen is a part of load-bearing. The organic matter pore can be compacted due to the soft framework. Besides, we consider the solid kerogen's fluid-like compressibility (Yan and Han, 2013), so

pore pressure increase will compress the solid kerogen to increase pore space. To satisfy the pore space volume equals the total volume of pore fluids, we have:

$$V_\phi(1+\beta_{pp}\Delta P)+V_k C_{om}\Delta P = V_{wi}(1-C_w\Delta P)+V_{HC}(1-C_{HC}\Delta P), \quad (13)$$

where V_ϕ, V_k, V_{wi}, and V_{HC} are volumes of pore, solid kerogen, initial water, and hydrocarbon, respectively. If the initial bulk volume is one, $V_\phi = V_T(\phi_k + \phi_{nk})$, $V_{wi} = \phi_{nk0}$, and $V_k = (1-\phi_{nk0})K_i(1-F)$. So we obtain

$$\Delta P = \frac{V_{wi}+V_{HC}-V_\phi}{V_\phi\beta_{pp}+V_k C_{om}+V_{wi}C_w+V_{HC}C_{HC}} . \quad (14)$$

In both cases, we utilize the pore compressibility upon pore pressure change, which can be calculated with solid phase K_0, drained frame stiffness K_d, and porosity ϕ for isotropic homogeneous medium (*Zimmerman*, 1991):

$$\beta_{pp} = [\frac{1}{K_d} - (1+\phi)\frac{1}{K_0}]/\phi . \quad (15)$$

The drained frame stiffness can be modeled while we conduct the rock physics modeling. Because the drained rock frame and the solid phase are modeled as TI mediums, their bulk modulus can be calculated by (*King*, 1964)

$$K_{TI} = \frac{C_{11}C_{33}-C_{33}C_{66}-C_{13}^2}{C_{11}-2C_{13}+C_{33}-C_{66}} . \quad (16)$$

Modeling Results and Discussion

If the density and compressibility of each component in equations 12 and 14 are irrelevant with pressure, the kerogen transformation ratio F and hydrocarbon expulsion ratio E control the pore pressure increase. Otherwise, we may use some numerical methods to solve the pore pressure if density and compressibility are pressure-dependent.

We take kerogen as pore-filling as an example and plot the pore pressure increase during the oil generation in Figure 5. Some input parameters include the non-kerogen-related porosity is 3%, and TOC is 2% before maturation. The results suggest that with increasing transformation ratio of kerogen or decreasing expulsion ratio of hydrocarbon, the generated pore pressure will increase. The ratio of ϕ_{nk} to V_k dominates the peak value. In Figure 6, two arrows denote how vertical P-wave velocity (km/s) and bulk density (g/cm³) of organic shale vary when transformation ratio of kerogen *(F)* or expulsion ratio of hydrocarbon *(E)* increases. During the oil generation, the velocity can decrease up to 0.2 km/s (6%), and density decreases trivially (~0.03 g/cm³ or 1%). An Increase in F decreases velocity because of the oil

generation and decreases density because of the increased porosity by pore pressure increase. Expulsion of oil increases shale density because the light component decreases. These characteristics are similar to the fluid expansion unloading model that velocity decreases and density seldom changes when pore pressure increases (Hoesni, 2004; Katahara, 2006; Ramdhan and Goulty, 2011).
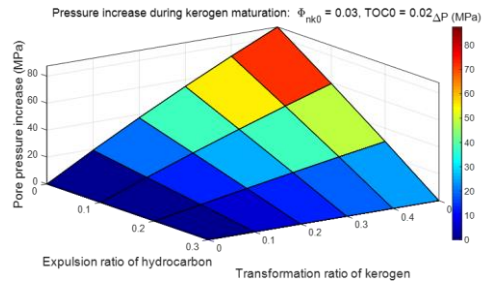

Figure 5. Pore pressure increase as a function of transformation ratio of kerogen (*F*) and expulsion ratio of hydrocarbon (*E*).
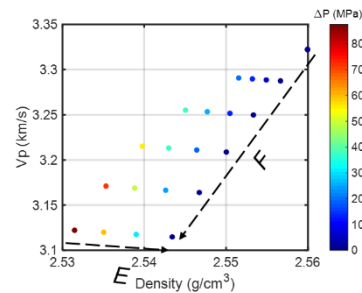

Figure 6. Modeled organic shale vertical P-wave velocity (km/s) vs. Density (g/cm3) with color-coded pore pressure increase.

For further work, we can consider the fracture pressure and the effects of fractures on elastic properties during hydrocarbon expulsion. We can improve the model by bridging the gap when TOC shifts from load-bearing to pore-filling during kerogen maturation. Pyrolysis experiments can be used to calibrate the model.

Conclusions

Our modeling results suggest that an increase in the transformation degree of kerogen or a decrease in the expulsion degree of hydrocarbon can increase the pore pressure in organic shale during its maturation. The volume ratio of pore water and the initial kerogen affects the peak pore pressure increase. The modeled elastic property variation in organic shale during kerogen maturation is consistent with fluid expansion model: velocity decreases and density changes little when pore pressure increases.

REFERENCES

Alfred, D., and L. Vernik, 2012, A new petrophysical model for organic-rich shales: SPWLA 53rd Annual Logging Symposium, 16–20.

Backus, G., 1962, Long-wave elastic anisotropy produced by horizontal layering: Journal of Geophysical Research, **67**, 4427–4440, https://doi.org/10.1029/JZ067i011p04427.

Berryman, J. G., 1980, Long-wavelength propagation in composite elastic media: The Journal of the Acoustical Society of America, **68**, 1809–1819, https://doi.org/10.1121/1.385171.

Carcione, J. M., H. B. Helle, and P. Avseth, 2011, Source-rock seismic-velocity models: Gassmann versus Backus: Geophysics, **76**, no. 5, N37–N45, https://doi.org/10.1190/geo2010-0258.1.

Ciz, R., and S. A. Shapiro, 2007, Generalization of Gassmann equations for porous media saturated with a solid material: Geophysics, **72**, no. 6, A75–A79, https://doi.org/10.1190/1.2772400.

Domenico, S. N., 1976, Effect of brine-gas mixture on velocity in an unconsolidated reservoir: Geophysics, **41**, 882–894, https://doi.org/10.1190/1.1440670.

Guo, Z., X. Li, C. Liu, X. Feng, and Y. Shen, 2013, A shale rock physics model for analysis of brittleness index, mineralogy and porosity in the Barnett Shale: Journal of Geophysics and Engineering, **10**, 025006, https://doi.org/10.1088/1742-2132/10/2/025006.

Hoesni, M. J., 2004, Origins of overpressure in the Malay Basin and its influence on petroleum systems: Ph.D. thesis, University of Durham.

Hornby, B. E., L. M. Schwartz, and J. A. Hudson, 1994, Anisotropic effective-medium modeling of the elastic properties of shales: Geophysics, **59**, 1570–1583, https://doi.org/10.1190/1.1443546.

Katahara, K., 2006, Overpressure and shale properties: Stress unloading or smectite-illite transition?: 76th Annual International Meeting, SEG, Expanded Abstracts.

King, M. S., 1964, Wave velocities and dynamic elastic moduli of sedimentary rocks: Ph.D. thesis, University of California.

Lucier, A. M., R. Hofmann, and L. T. Bryndzia, 2011, Evaluation of variable gas saturation on acoustic log data from the Haynesville Shale gas play, NW Louisiana, USA: The Leading Edge, **30**, 300–311, https://doi.org/10.1190/1.3567261.

Milliken, K. L., M. Rudnicki, D. N. Awwiller, and T. Zhang, 2013, Organic matter-hosted pore system, Marcellus Formation (Devonian), Pennsylvania: AAPG Bulletin, **97**, 177–200, https://doi.org/10.1306/07231212048.

Nishizawa, O., 1982, Seismic velocity anisotropy in a medium containing oriented cracks: Journal of Physics of the Earth, **30**, 331–347, https://doi.org/10.4294/jpe1952.30.331.

Qin, X., D. Han, and L. Zhao, 2014, Rock physics modeling of organic-rich shales with different maturity levels: 84th Annual International Meeting, SEG, Expanded Abstracts.

Ramdhan, A. M., and N. R. Goulty, 2011, Overpressure and mudrock compaction in the Lower Kutai Basin, Indonesia: A radical reappraisal: AAPG Bulletin, **95**, 1725–1744, https://doi.org/10.1306/02221110094.

Sayers, C. M., 1994, The elastic anisotropy of shales: Journal of Geophysical Research, **99**, 767–774, https://doi.org/10.1029/93JB02579.

Sone, J., and M. D. Zoback, 2013, Mechanical properties of shale-gas reservoir rocks—Part 1: Static and dynamic elastic properties and anisotropy: Geophysics, **78**, no. 5, D381–D392, https://doi.org/10.1190/geo2013-0050.1.

Tosaya, C. A., 1982, Acoustical properties of clay-bearing rocks: Ph.D. thesis, Stanford University.

Vernik, L., and J. Milovac, 2011, Rock physics of organic-rich shales: The Leading Edge, **30**, 318–323, https://doi.org/10.1190/1.3567263.

Yan, F., and D. Han, 2013, Measurement of elastic properties of kerogen: 83rd Annual International Meeting, SEG, Expanded Abstracts, 2778–2782.

Zhao, L., X. Qin, D. Han, J. Geng, Z. Yang, and H. Cao, 2016, Rock-physics modeling for the elastic properties of organic shale at different maturity stage: Geophysics, **81**, no. 5, D527–D541, https://doi.org/10.1190/geo2015-0713.1.

Zhu, Y., S. Xu, M. Payne, A. Martinez, E. Liu, C. Harris, and K. Bandyopadhyay, 2012, Improved rock-physics model for shale gas reservoirs: 82nd Annual International Meeting, SEG, Expanded Abstracts.

Zimmerman, R. W., 1991, Compressibility of sandstones: Elsevier.